Precision measurement of the muon momentum in pion decay at rest

M. Daum, G. H. Eaton, R. Frosch, H. Hirschmann, J. McCulloch,* R. C. Minehart,† and E. Steiner
Swiss Institute for Nuclear Research, SIN, 5234 Villigen, Switzerland
(Received 26 June 1979)

At the Schweizerisches Institut für Nuklearforschung (SIN) we have measured the muon momentum in the pion decay $\pi^+ \to \mu^+ + \nu_\mu$ at rest using a magnetic spectrometer. Our result is $p_{\mu^+} = 29.7877 \pm 0.0014$ MeV/c. From our p_{μ^+} value and the rest masses of the muon, $m_{\mu^+} = 105.65946 \pm 0.00024$ MeV/c^2, and the pion, $m_{\pi^-} = 139.5679 \pm 0.0015$ MeV/c^2, we derive a new value for the squared muon-neutrino rest mass, $m_{\nu_\mu}{}^2 = 0.13 \pm 0.14$ (MeV/c^2)^2. From this we obtain $m_{\nu\mu} \leq 0.57$ MeV/c^2 (90% C.L.), which is at present the lowest experimental upper limit for the muon-neutrino rest mass. Here the validity of the *CPT* theorem ($m_{\pi^+} = m_{\pi^-}$) and energy and momentum conservation in pion decay were assumed. Our result can be interpreted in a second way: From cosmological arguments using the big-bang hypothesis an upper limit of about 40 eV/c^2 has been derived for the neutrino rest mass. With this limit and the above value of the muon mass we can calculate the pion-muon mass difference or the rest mass of the π^+ with strongly improved precision from our measurement. The results are $\delta m = m_{\pi^+} - m_{\mu^+} = 33.9063 \pm 0.0018$ MeV/c^2 or $m_{\pi^+} = 139.5658 \pm 0.018$ MeV/c^2. This positive-pion mass is consistent with the present world average for the negative-pion mass, in agreement with the *CPT* theorem.

I. INTRODUCTION

The aim of the present experiment was the precision measurement of the muon momentum p_{μ^+} in the most frequent pion decay, $\pi^+ \to \mu^+ \nu_\mu$, at rest, with the main purpose of contributing to a more precise determination of the muon-neutrino rest mass. In a conventional two-component neutrino theory with muon-number conservation, the muon-neutrino mass is predicted to be zero. However, in the more recent unified theories of weak and electromagnetic interactions, violations of muon-number conservation and finite neutrino masses are not excluded. Furthermore, the neutrino masses play an important role in cosmology. If the mean lifetime of the muon neutrino is assumed to be greater than or about equal to the age of the universe, its rest mass can be determined with "big-bang" model calculations[1,2] from the present deceleration parameter to be below about 40 eV. Laboratory measurements of m_{ν_μ} serve as tests of the assumptions made in the cosmological calculations.

All neutrino-mass experiments have so far given values compatible with zero. The rest mass of the electron antineutrino has been measured most precisely by Tret'yakov *et al.*[3] From a study of the upper end of the electron spectrum in tritium β decay they found an upper limit of 35 eV for $m_{\bar{\nu}_e}$. The measurements of m_{ν_μ} have so far been much less accurate. The world average of p_{μ^+} before our experiment, 29.794 ± 0.010 MeV/c, gave an upper limit of m_{ν_μ} around 1.0 MeV/c^2. Clark *et al.*[4] have determined m_{ν_μ} from the upper end of the invariant $(\pi^\pm\mu^\mp)$ mass distribution in the decay $K_L^0 \to \pi^\pm\mu^\mp\nu$; they find an upper limit of 0.65 MeV/c^2 (90% C.L.) for m_{ν_μ}. In their analysis, the $(\pi^\pm\mu^\mp)$ mass distribution is fitted with curves derived under the assumption of the exact validity of the $V-A$ theory for the K_L^0 decay.

The large difference between the upper limits for $m_{\bar{\nu}_e}$ and m_{ν_μ} can be understood by considering that the ideal decay process for the determination of a neutrino mass must satisfy three conditions:

(a) The kinetic energy of the observed charged particle must be small, so that the absolute uncertainty of the measured energy is small,

(b) the momentum of the neutrino must be small (zero if possible) so that the neutrino energy depends strongly on its rest mass, and

(c) the decay process must occur with a sufficiently large branching ratio.

All three conditions are well satisfied for tritium β decay near the end point, whereas in the case of the muon neutrino no similarly advantageous process has been found; e.g., the decay $K_L^0 \to \pi^\pm\mu^\mp\nu$ studied in Ref. 4 is suitable concerning conditions (b) and (c) but not (a), whereas the decay $\pi^+ \to \mu^+\nu_\mu$ at rest, used in our experiment, adequately satisfies conditions (a) and (c) but not (b); the neutrino has a momentum of about 29.8 MeV/c and therefore its energy depends only weakly on m_{ν_μ}.

As a starting point for our experiment we chose the 1967 measurement of Booth *et al.*[5] where the pions were stopped in a small scintillator and the muon momenta were measured with a magnetic spectrometer. The largest contribution to the p_{μ^+} uncertainty of Ref. 5 was statistical and could easily be reduced at SIN. The second largest contribution to Δp_{μ^+} in Ref. 5 came from the uncertainty in the absolute calibration of the spectrometer. This we improved by replacing the inhomogeneous

magnetic field of their spectrometer by a homogeneous field which can be accurately mapped and monitored with nuclear-magnetic-resonance probes.

II. KINEMATICS

Our experiment is based on the kinematics of the decay $\pi^+ \to \mu^+ \nu_\mu$ at rest. From energy and momentum conservation one obtains

$$m_{\nu_\mu}{}^2 = m_{\pi^+}{}^2 + m_{\mu^+}{}^2 - 2m_{\pi^+}(p_{\mu^+}{}^2 + m_{\mu^+}{}^2)^{1/2}, \quad (1)$$

where p_{μ^+} is the momentum of the muon ($c = 1$). In Fig. 1 the muon momentum p_{μ^+} calculated from Eq. (1) is plotted as a function of the assumed neutrino mass m_{ν_μ}. The values of m_{μ^+} and m_{π^-} were taken from the compilation of the Particle Data Group (PDG).[6] We have assumed the validity of the CPT theorem and set m_{π^+} equal to m_{π^-}. Since p_{μ^+} depends only weakly on m_{ν_μ} for small m_{ν_μ}, a large reduction of the upper limit on m_{ν_μ} is difficult.

According to Eq. (1) the possible reduction of the uncertainty $\Delta(m_{\nu_\mu}{}^2)$ is limited by the uncertainties of m_{π^+} and m_{μ^+}. Differentiation of Eq. (1) leads, for small $m_{\nu_\mu}{}^2$, to the following sensitivities:

$$\frac{\partial(m_{\nu_\mu}{}^2)}{\partial m_{\pi^+}} = \frac{m_{\pi^+}{}^2 - m_{\mu^+}{}^2}{m_{\pi^+}} = 59.6 \text{ MeV}, \quad (2)$$

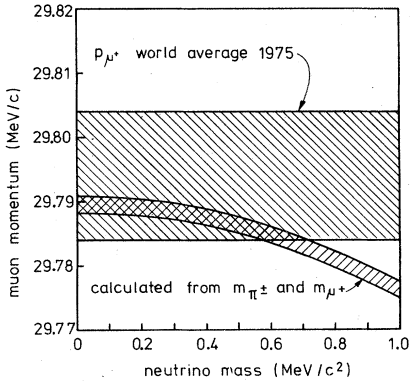

FIG. 1. Muon momentum p_{μ^+} in stopped-pion decay as a function of the neutrino rest mass m_{ν_μ}. Curved band: p_{μ^+} calculated using Eq. (1) from the Particle Data Group mass values (Ref. 6), $m_{\mu^+} = 105.659\,46 \pm 0.000\,24$ MeV/c^2 and $m_{\pi^-} = 139.5679 \pm 0.0015$ MeV/c^2 assuming that $m_{\pi^+} = m_{\pi^-}$ (CPT theorem). Straight horizontal band: experimental value of p_{μ^+} (world average 1975). The widths of the bands correspond to the uncertainties (± 1 standard deviation). The region of allowed values for m_{ν_μ} is approximately given by the overlap of the two bands. As the two bands become parallel for $m_{\nu_\mu} \to 0$, the upper limit of m_{ν_μ} decreases only weakly with the uncertainties of p_{μ^+}, $m_{\pi^\pm}$, and m_{μ^+}.

$$\frac{\partial(m_{\nu_\mu}{}^2)}{\partial m_{\mu^+}} = -2m_{\mu^+}\frac{m_{\pi^+}{}^2 - m_{\mu^+}{}^2}{m_{\pi^+}{}^2 + m_{\mu^+}{}^2} = -57.3 \text{ MeV}, \quad (3)$$

$$\frac{\partial(m_{\nu_\mu}{}^2)}{\partial p_{\mu^+}} = -2m_{\pi^+}\frac{m_{\pi^+}{}^2 - m_{\mu^+}{}^2}{m_{\pi^+}{}^2 + m_{\mu^+}{}^2} = -75.7 \text{ MeV}. \quad (4)$$

The three differentials are of similar magnitude; it is therefore reasonable to measure p_{μ^+} with about the same absolute uncertainty (in MeV; $c = 1$) as the less accurate of the two particle masses involved. The uncertainty[6] of m_{π^-} is 0.0015 MeV, so the p_{μ^+} uncertainty to be obtained is $\lesssim 0.0015$ MeV/c.

III. EXPERIMENTAL METHOD

The experimental arrangement for the p_{μ^+} measurement is shown in Fig. 2. Positive pions with momentum $p_\pi = 200$ MeV/c from the SIN $\pi E1$ high-intensity channel[7] enter the spectrometer magnet gap, are slowed down in a degrader, and pass through a vacuum window. A fraction of the pions stop in a small scintillator. The pions of interest are those which come to rest close to the downstream face of the scintillator, because their decay muons can leave the scintillator with little or no energy loss. A muon which is created at the scintillator surface and which starts along the central trajectory of the spectrometer travels along this trajectory if the magnetic field is about 2760 G. It is identified at the end of the trajectory with a silicon surface barrier detector. At higher magnetic fields one expects the muon rate to decrease to zero, while at lower field values, muons are detected which come from a finite depth of the scintillator, and therefore lose a small part of their energy in leaving the scintillator.

Our data-taking runs consisted of registering the pulse-height spectrum of the silicon counter gated by pions stopping in the scintillator, for each of a series of magnetic-field values closely spaced about that field region for which muons with the full decay momentum p_{μ^+} are accepted by the spectrometer. In principle, the momentum p_{μ^+} was determined from the magnetic-field value at which the drop in the good-event rate occurred.

IV. THE APPARATUS

A. The pion beam

The SIN channel $\pi E1$ used for our experiment has one of the most intense medium-energy pion fluxes.[7,8] The pions are produced by 588-MeV protons from the ring accelerator, normally in a 22-g/cm^2-thick beryllium target. The acceptance solid angle of the channel is 50 msr and the maximal accepted momentum band is 10% [full width

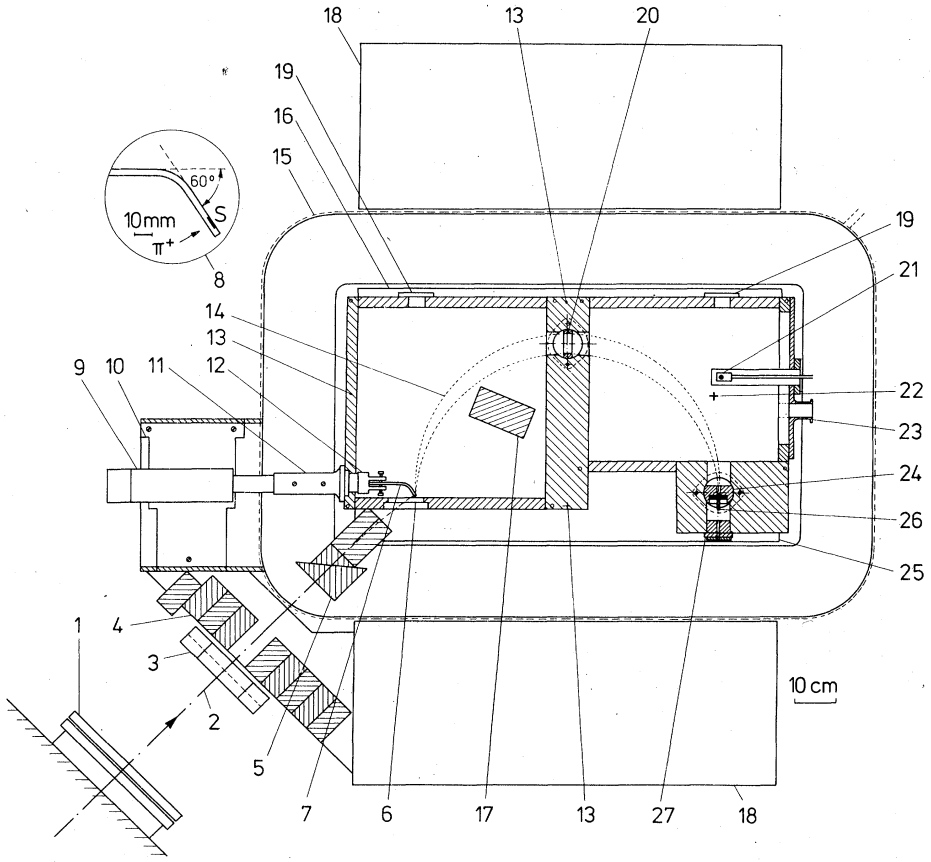

FIG. 2. Experimental arrangement for the muon momentum measurement: (1) exit vacuum window of the pion channel, (2) central trajectory of the pion beam, (3) multiwire proportional chamber for beam profile measurements, (4) lead collimator, (5) remotely controlled pion degrader (polyethylene and graphite), (6) window of the spectrometer vacuum chamber, (7) light guide of the pion-stop scintillation counter S, (8) enlarged view of the counter S, (9) photomultiplier of the counter S, (10) adjustable support of the photomultiplier, (11) vacuum feedthrough of the light guide, (12) positioning mechanism for the scintillator S, (13) vacuum chamber of the spectrometer (aluminum), (14) region of accepted muon trajectories, (15) correction coils for magnetic-field stabilization, (16) pole of the magnet, (17) lead beam stopper, (18) yoke of the magnet, (19) ports for glass windows used during optical measurements of scintillator and collimator position, (20) copper collimator B, (21) Nuclear-magnetic-resonance probe for magnetic-field measurement and stabilization, (22) ^{241}Am α source for calibration of the silicon detector, (23) port for vacuum pump, (24) copper collimator C, (25) magnet coils, (26) silicon surface barrier detector (Si) for muon detection, (27) coaxial vacuum feedthrough for the counter Si.

at half maximum (FWHM)]. The total pion rate at $p_{\pi^+} = 200$ MeV/c at the end of the 14-m-long channel was 1×10^9 π^+/sec for a proton beam of 35 μA (typical value when most of our data were taken). The pion-stop density under these conditions at the end of the pion degrader (Fig. 2) was about 5×10^6 stops/(g sec), whereas in the pion-stop counter, 10 cm after the downstream face of the degrader, the stop density was only 1×10^6 stops/(g sec) because of the strong divergence of the pion beam leaving the degrader.

B. The scintillation counter

The NE102A scintillation counter S used as the

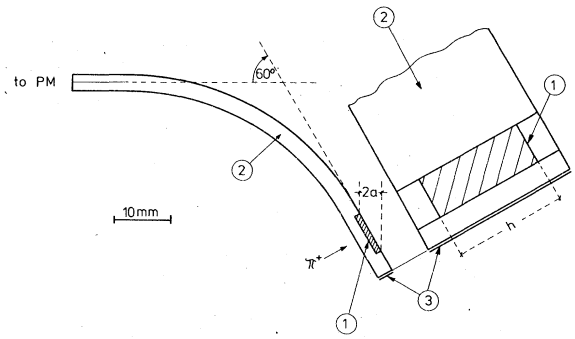

FIG. 3. The scintillation counter S. (1) NE102A scintillator, (2) Lucite light guide, (3) aluminum reflector.

source of muons is shown in Fig. 3. The position of the scintillator in the homogeneous magnetic field of the spectrometer is shown in Fig. 2, together with the Lucite light guide and the photomultiplier. Our method requires that the shape of the effective muon source differs only slightly from that of the scintillator. In order to satisfy this requirement, the scintillator was placed perpendicular to the trajectory of interesting pions; it was glued in a 1-mm-deep groove in the light guide such that a smooth polished surface could be obtained, and the usual aluminum wrapping was omitted on the downstream face.

The uniformity of response across the face of the scintillator was tested with a narrowly collimated ^{90}Sr β source. Near the center of the scintillator about 50 photoelectrons were produced from the photocathode of the photomultiplier per MeV of energy deposited in the scintillator, and this number was seen to be constant to $\pm 1\%$ across the whole face of the scintillator, excluding a narrow fringe close to the edges where the average pulse height was reduced because of the shorter average path length of the electrons in the scintillator. This effect is present also for pions and has been taken into account in our analysis (Sec. VIII D).

The height and width of the scintillator were chosen to match the dimensions of the spectrometer collimators (see Sec. IV C). The thickness of the scintillator (1 mm) was dictated by the requirement that there be as few accidental triggers as possible, and therefore as few scintillator counts per good muon event as possible.[8]

C. The muon collimators

The muon collimators B and C (Fig. 2) have been made of a high-density material, so that the opening is accurately defined by the collimator jaws. For ease of accurate machining we chose copper; the range of 4.12-MeV muons in Cu is only 0.25 mm. The slit scattering was appreciable and had to be considered in the analysis (Sec. VIII B).

The radius ρ_0 of the central muon trajectory in the spectrometer was 360 mm. The height of the collimator openings was chosen equal to that of the scintillator, $h = 20$ mm. The inner height of the vacuum chamber was 65 mm on both sides of the collimator B (Fig. 2). This is large enough to prevent muons created in the scintillator from getting through both collimators by a single scattering on the top or bottom of the aluminum vacuum chamber.

The widths of the collimators and the scintillator were optimized for maximal muon event rate for a given momentum acceptance of the spectrometer.[8] The width of the momentum acceptance curve was 0.64% (FWHM) in the first half of the experiment and 0.39% (FWHM) in the second half. The two corresponding resolution curves are shown in Fig. 4. The accepted momentum bands (FWHM) mentioned above were chosen to be about 100 times larger than the desired p_{μ^+} uncertainty (standard deviation). This represented the usual compromise between the requirements of large enough event rate on one hand and small enough linewidth, and therefore small enough theory dependence, on the other hand. We thus chose the widths $2a = 4$ mm (2.5 mm) and $2b = 54$ mm (42 mm) for the first (second) part of the data taking; here $2a$ is both the projected width of the muon source and the horizontal opening of the second collimator, and $2b$ is the horizontal opening of the first collimator; see Fig. 2. The corresponding scintillator widths were 8 mm (5 mm), see Fig. 3. With the height h and the radius ρ_0 fixed, the accepted solid angle of the spectrometer is found to increase as $(\Delta p/p_0)^{1/2}$ and the muon event rate (for magnetic-field values below the edge) increases as $(\Delta p/p_0)^{5/2}$ if the pion-stop density in the scintillator is kept fixed.[8]

D. The muon detector

The muon counter was a commercial silicon surface barrier detector, placed immediately be-

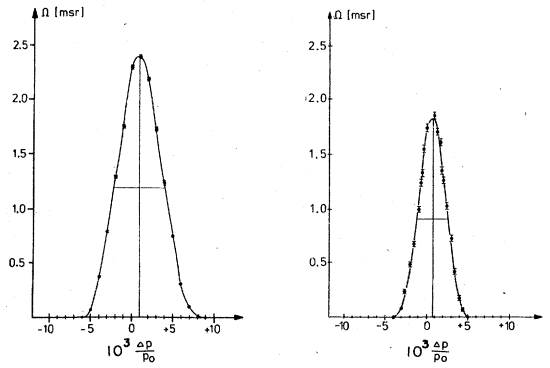

FIG. 4. Resolution curves of the spectrometer determined with a Monte Carlo computer program. Abscissa: Deviation of the particle momentum p from the momentum p_0 for the central trajectory, as a fraction of p_0. Ordinate: Effective acceptance solid angle, in msr. For the graph on the left the source width (cf. Fig. 3) and the horizontal opening of collimator C (cf. Fig. 2) were both $2a = 4$ mm and the horizontal opening of collimator B was $2b = 54$ mm. For the graph on the right the dimensions were $2a = 2.5$ mm and $2b = 42.4$ mm. The points represent the results of the Monte Carlo program; the curves have been drawn to guide the eye. The widths of the two curves are 6.4×10^{-3} and 3.9×10^{-3} (FWHM).

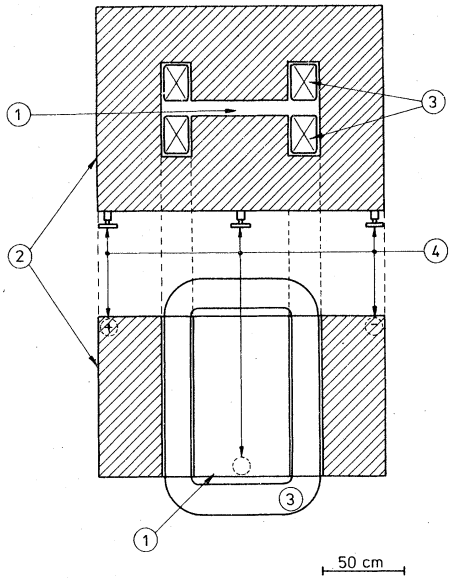

FIG. 5. The standard SIN bending magnet (type ASL) used as spectrometer (cf. Fig. 2). (1) pole gap, (2) yoke, (3) coils, (4) adjustable supporting legs.

hind the collimator C (Fig. 2). The electrode diameter was 20 mm and the thickness of the depletion layer was 1 mm. The accepted muons had a kinetic energy below 4.12 MeV and were stopped in the depletion layer. Therefore they produced a narrow line in the pulse-height spectrum of the detector and could be separated clearly from the background.

The detector was placed inside the homogeneous magnetic-field region of the spectrometer. The detector was scanned with a collimated ^{90}Sr source; the pulse height was found to vary less than 0.5% across the face of the detector.

E. The magnet

We have used a semicircular magnetic spectrometer with homogeneous field.[9] As the magnet (see Fig. 5) is a standard SIN beam transport element,[10] its field homogeneity was originally insufficient for our purposes. The shims that we attached to the pole surfaces are described in Refs. 8 and 11. In Fig. 6 a partial field map in the midplane of the shimmed magnet is shown. In the crescent-shaped region of the muon trajectories the field is constant to about ±0.15 G. Before the shimming there had been variations of ±1.5 G.

During the data-taking runs a fixed NMR probe was installed at point R (Fig. 6). For a given point of the muon spectrum the reading of this reference probe was automatically kept constant using a feedback loop connecting the NMR device to correction coils on the magnet (Fig. 2). Between

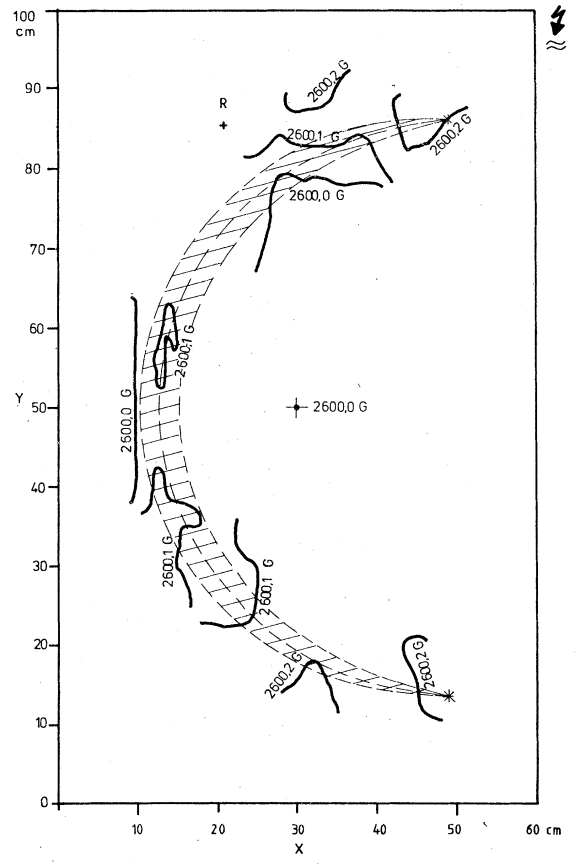

FIG. 6. Lines of constant magnetic field in the midplane of the shimmed ASL magnet (see Fig. 5). During the data taking a fixed nuclear-magnetic-resonance probe used for magnetic-field stabilization was placed at point R. The accepted muon trajectories lie in the indicated crescent-shaped region.

runs the complete field map was measured with a second, movable NMR probe. During these field mappings the reference probe, which served to keep the field constant in time, was moved away from point R (Fig. 6), so that the field map in the crescent as well as the field at point R could be measured with the same probe. All field maps obtained were combined to give the relation $B_{\mathrm{eff}} - B(R) = 0.065 \pm 0.005$ G; here, $B(R)$ is the field at point R which for the field mapping was kept near 2750 G, and B_{eff} is defined as follows: As shown by Hartree[12] a spectrometer of our type with an imperfectly homogeneous field has the same mean accepted momentum as a spectrometer with the same source and collimators and the homogeneous field B_{eff} if

$$B_{\mathrm{eff}} = \tfrac{1}{2} \int_0^{\pi} \bar{B}(\theta) \sin\theta \, d\theta \, ; \tag{5}$$

here, θ is the angle defined by a point P on the central trajectory, the center M of the central

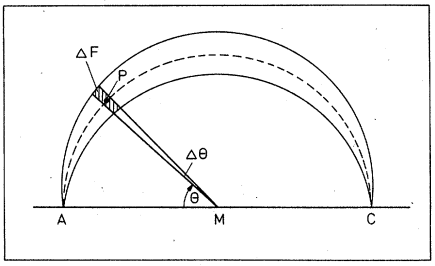

FIG. 7. For the calculation of the effective magnetic field B_{eff} according to Hartree (Ref. 12) the field $\bar{B}(\theta)$ needed for Eq. (5) was set equal to the average of the field strength over the volume with area ΔF, as indicated in this figure, and height $h = 2$ cm. The area ΔF is defined by the crescent-shaped region of accepted muon trajectories (cf. Fig. 2).

trajectory, and the source center A, see Fig. 7. For $\bar{B}(\theta)$ we used the average of the field strength over the volume with area ΔF (Fig. 7) and height $h = 2$ cm. This procedure was checked by comparing the momentum-resolution curve obtained from a Monte Carlo computer program using a typical field map with that derived from a constant field B_{eff}. The resulting relative momentum differences were smaller than 1.5 ppm and thus negligible compared to the required p_{μ^+} uncertainty of 50 ppm. Using a constant field B_{eff} rather than a complete field map significantly reduced the computer time for the final analysis program.

F. The magnetic-field measurement system

The measurement of the magnetic field at the fixed reference point in the magnet was done with a commercial nuclear-magnetic-resonance sys-

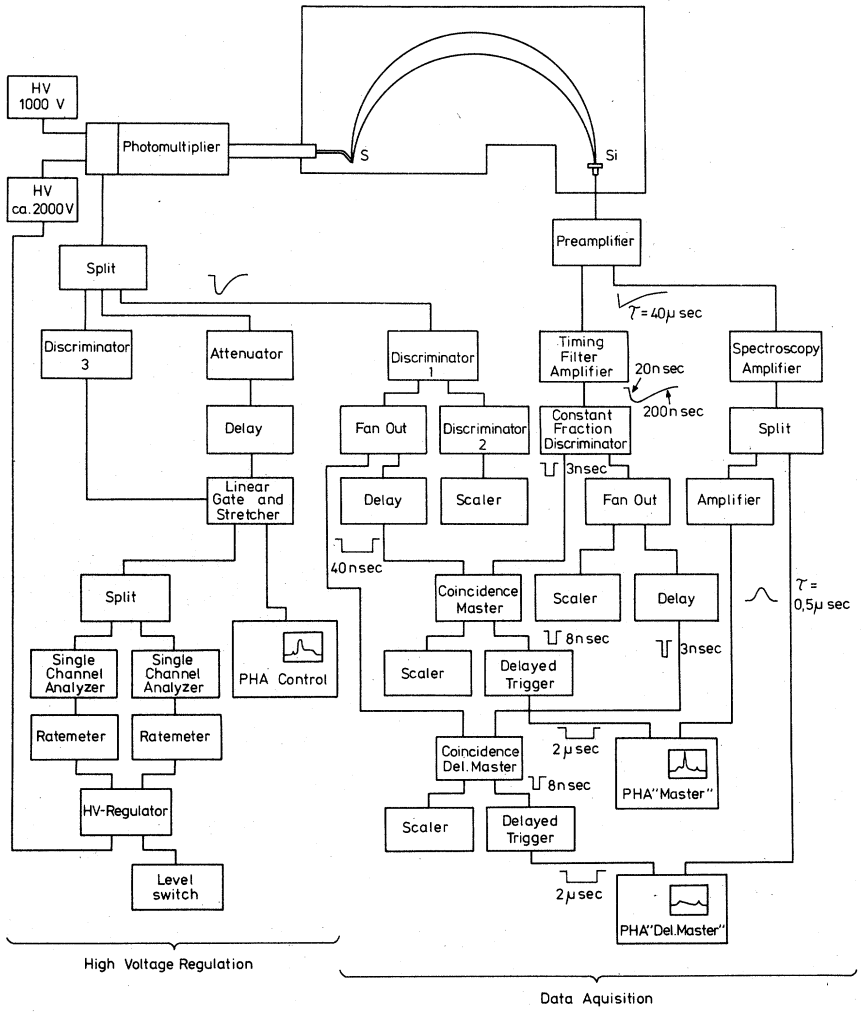

FIG. 8. Diagram of the data-taking electronics, see text (Sec. IV G).

tem.[8] This system was guaranteed by the manufacturer to an absolute precision of 6×10^{-6} (standard deviation) and was chosen because of its suitability for the relatively low magnetic field in the experiment. This system was checked at a nominal field of 2760 G with another commercial NMR system. The two systems differed by 0.03 G (1.1×10^{-5}). As the first system was especially selected and optimized for the field strengths used in our experiment, we adopted its values with the uncertainty given by the manufacturer for our analysis.[8]

G. The electronics

The data-taking electronics had to process signals from two particle detectors only. Thus the electronics, which is shown in Fig. 8, could be kept comparatively simple. A pion which travels through the total thickness of the scintillator (1 mm) and then stops loses about 3.6 MeV in the scintillator. A signal from the scintillator was accepted by discriminator 1 (Fig. 8) as a pion-stop signal if its height corresponded to an energy loss of more than 3.0 MeV. Most of the nonstopped pions passing through the scintillator lose too little energy in it to create such a signal. Selecting large signals from this stop counter alone was preferred to the more conventional system with an anticounter because at our high pion fluxes an anticounter would accidentally veto a large fraction of the good triggers.

In order to serve as a stable monitor the pion counter had to have automatic pulse-height stabilization. The regulation unit (Fig. 8) kept the ratio of the rates from two single-channel analyzers (SCA) fed by the photomultiplier (PM) at a constant value. The two SCA's were set on either side of a sharp edge observed in the pulse-height spectrum at a pulse height corresponding to an energy loss of about 7 MeV in the counter. The edge is caused by pions and corresponding decay muons both being stopped in the scintillator; the two signals are summed in the SCA's and give a pulse-height distribution reaching up to about 7.7 MeV.

For the coincidence timing with the pulses from the silicon detector (Si), discriminator 1 was used to generate gating pulses of 40-nsec length. True pion-decay events were selected by demanding a coincidence between the Si pulse and a scintillator (S) pulse generated 24 to 64 nsec before the Si event. This timing criterion eliminated prompt coincidences (scattered pions, muons from pion decay in flight, etc.); the flight time of the muons in the spectrometer from S to Si was 14 nsec. The accidental spectrum of events in Si was derived from the coincidence between an Si pulse and an S pulse generated 56 to 96 nsec after the Si event. The output of these coincidence circuits labeled MASTER and DELMASTER, respectively, were used as separate electronic gates to the two pulse-height analyzers shown in Fig. 8. These accumulated and displayed the pulse-height spectra for the two different types of events. The DELMASTER spectrum was used to calculate the accidental background in the pulse-height distribution of the coincidence events in the silicon counter.

V. THE EXPERIMENTAL MUON SPECTRA

Typical pulse-height spectra obtained with the silicon detector in one of our data-taking runs are presented in Fig. 9. Part (a) of this figure contains the spectrum of the coincidence (MASTER)

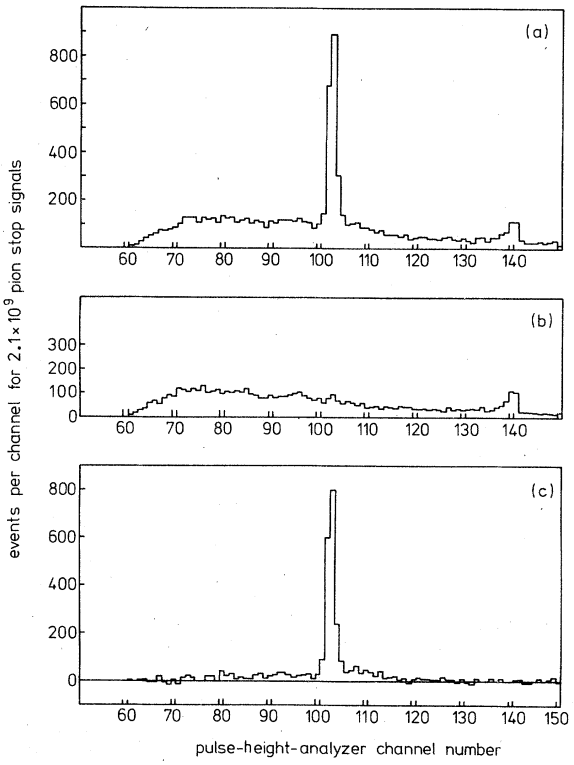

FIG. 9. Pulse-height spectra from the silicon detector recorded at a magnetic field of 2740.1 G. (a) Spectrum obtained with the MASTER pulse-height analyzer (see Fig. 8). Here the Si-counter signals were gated by coincidence pulses, as described in Sec. IV G. (b) Spectrum due to accidental coincidences derived from the DELMASTER pulse-height-analyzer data. (c) Difference (a) – (b); spectrum due to nonaccidental coincidences. The peak centered on Channel 103 arises from decay muons born in the scintillator which are accepted at this magnetic-field value (average $T_{\mu^+} = 4.07$ MeV); the peak around channel 140 is generated by α particles from the ^{241}Am calibration source ($T_\alpha = 5.48$ MeV). Details of the spectra are discussed in Sec. V.

pulse-height analyzer; part (b) contains the spectrum due to accidental coincidences derived from the DELMASTER pulse-height analyzer spectrum; part (c) is the difference (a) – (b), i.e., the spectrum due to nonaccidental coincidences.

The narrow peak in channel 103 is produced by good muons from stopped pion decays in the scintillator. The peak in channel 140 is produced by α particles from the ^{241}Am source. This peak is not present in Fig. 9(c) as expected, because the corresponding triggers were accidental coincidences of an α event in the Si counter with a signal in the scintillator. Using the α line for calibration one can verify that the peak in channel 103 is indeed generated by muons accepted at $B = 2740$ G ($p_{\mu^+} = 29.6 \pm 0.1$ MeV/c).

The shoulder in Fig. 9(c), in channels 105 to about 120, is due to the $(\mu + e)$ events, i.e., to the cases where the positron from the muon decay made a contribution to the Si counter pulse height. This shoulder was included in the good-event count; the number of good events was calculated by summing the events in channels $(I - 3)$ to $(I + 16)$, where I is the channel number of the muon peak ($I = 103$ in the case of Fig. 9). Replacing the upper limit $(I + 16)$ by $(I + 3)$ had a negligible effect on the p_{μ^+} result. In Fig. 9(c) there is a flat pulse-height distribution to the left of the muon peak in channels 70 to 100. This distribution is produced by muons scattered in the collimators and had to be excluded from the good events. The subtraction of the background due to scattered muon events in the peak [e.g., above channel 100 in the case of Fig. 9(a)] is discussed in Sec. VIII B. The spectra of Fig. 9 are empty below channel number 60 because of pulse-height discrimination in the constant fraction discriminator (Fig. 8).

Figure 10 is analogous to Fig. 9; however, the magnetic field in the case of Fig. 10 was so high that almost no good muons reached the silicon counter. The number of scattered muons in the spectrum of Fig. 10(c) is consistent with zero.

In Fig. 11 the number of good muons is plotted as a function of the magnetic field for all our data. The spectra obtained in the same data-taking period and therefore with the same spectrometer geometry were combined. Before combining the

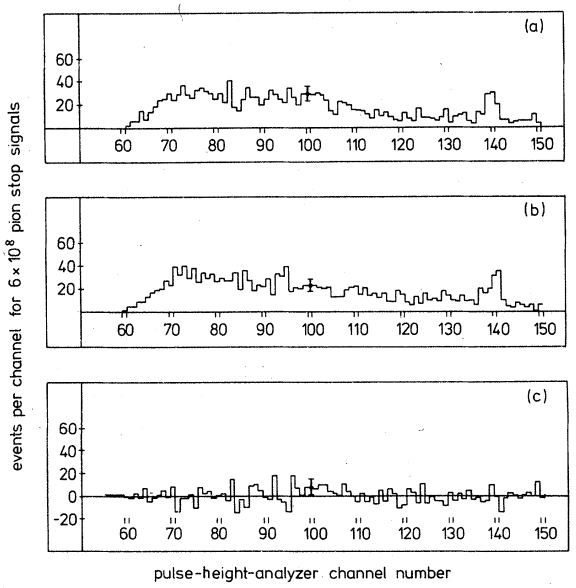

FIG. 10. Same as Fig. 9, but for a magnetic field of 2772.6 G. At this field almost no good muons can reach the silicon detector; therefore, the peak near channel 104 is much smaller than in Fig. 9.

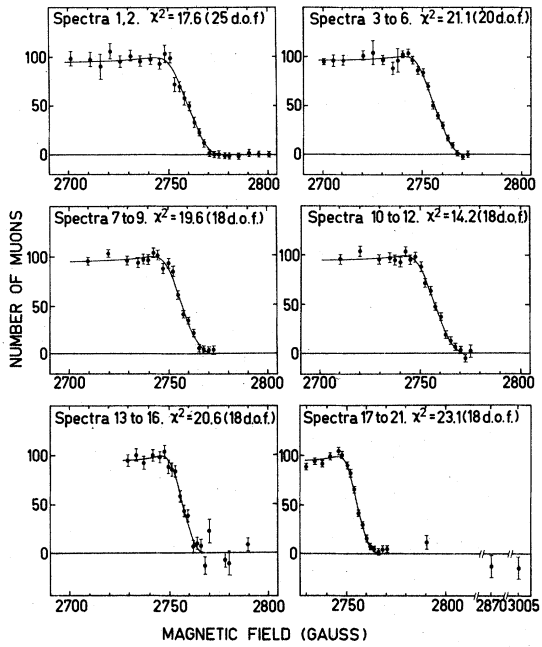

FIG. 11. Muon spectra obtained during the six data-taking periods of the experiment. Abscissa: Magnetic field at the reference point R (Fig. 6). Ordinate: Number of muons in the silicon-detector pulse-height spectrum, after background subtraction, normalized to 100 events at the maximum of the theoretical curve (see Sec. V). The points with error bars represent the experimental data; the solid lines are the fitted theoretical curves. The χ^2 values of the fits are indicated in the figure. In the last two of the six spectra the cutoff is sharper because the momentum acceptance of the spectrometer was smaller than for the earlier spectra. The theoretical curve is slightly different for each of the six spectra because of changes of the scintillator position made between runs. After the normalization of the ordinate there was for each of the six spectra only one additional free parameter, namely, a horizontal shift, i.e., the value of the decay muon momentum.

21 individual spectra into the six spectra of Fig. 11, the ordinate of each was stretched or compressed so that the maximum of the theoretical curve (Sec. VI) was $N_{\mu}^{\max}=100$. This was done because the discrimination level of the scintillation counter had in some cases been deliberately changed before recording the next spectrum; therefore, the number of good muons per scintillator signal at a given magnetic field changed from one spectrum to the next, and the scintillation counter could not be treated as an absolute monitor. The final value for $p_{\mu+}$ was derived from the 21 individual spectra (Sec. IX).

It is seen from Fig. 11 that the good-event rate varies with magnetic field in the expected way; i.e., the rate is roughly constant up to a cutoff field near 2750 G, then drops sharply and is consistent with zero for higher fields.

VI. THE THEORETICAL MUON SPECTRA

The theoretical muon spectra, which were to be fitted to the data of Fig. 11, were generated from the initial assumption of a free-muon momentum of 29.7900 MeV/c with a Monte Carlo computer program.

The input for this program was

(a) the spatial distribution of those stopped pions which had made a large enough signal (energy loss ≥ 3.0 MeV) in the scintillator, see Sec. VIII D,

(b) the effective magnetic field (see Sec. IV E),

(c) size and position of the scintillator, the collimators, and the silicon detector (Sec. IV), and

(d) energy loss and multiple scattering of the muons in the scintillator.

First the position of the pion decay in the scintillator and the muon momentum vector were generated. Then the path length Δl of the muon in the scintillator was computed. The energy loss of the muon on the path Δl was generated from collision loss theory (see Sec. VIII C). The resulting momentum spectrum of muons leaving the scintillator approximately in the good direction is presented in Fig. 12. Here the free muon momentum was set to 29.79 MeV/c. The spectrum of Fig. 12 cuts off sharply at this value, and is approximately flat for lower momenta. The peak just below the cutoff is due to the smallness of the momentum-loss straggling for small path lengths. Momentum bins near the cutoff lose few muons by straggling, but gain many from straggling for muons with longer paths.

The number of Monte Carlo muons passing both collimators and hitting the silicon detector is plotted in Fig. 13 as a function of the assumed homogeneous magnetic field B_{eff}. As mentioned already, the computer time used for the Monte Carlo program was fairly long; so the number of Monte Carlo events was only increased until the $p_{\mu+}$ uncertainty, due to Monte Carlo statistics, was as low as 15% of the total $p_{\mu+}$ uncertainty. The results obtained with the program for one of the six data-taking periods are plotted as points with er-

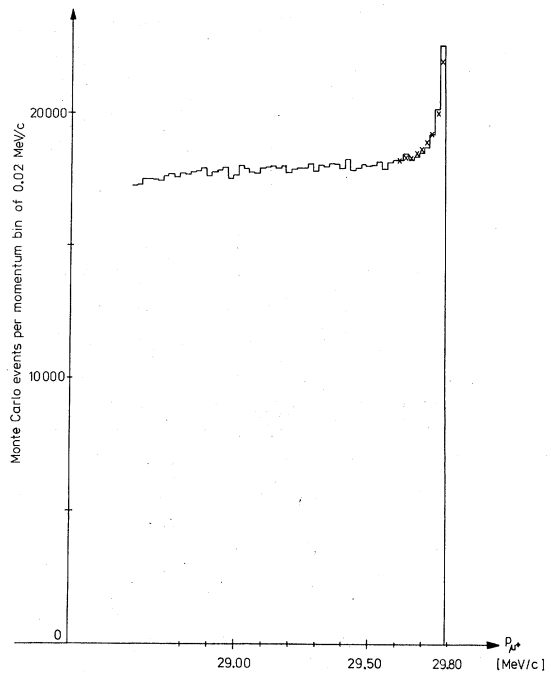

FIG. 12. Predicted momentum spectrum of muons leaving the scintillator approximately in the "good" direction. A decay momentum of 29.79 MeV/c was assumed for this Monte Carlo calculation. The muon energy loss in the scintillator has been generated from the distributions of Shulek *et al.* (Ref. 15) (solid line) or Vavilov (Ref. 14) (crosses), see Sec. VI and VIII C.

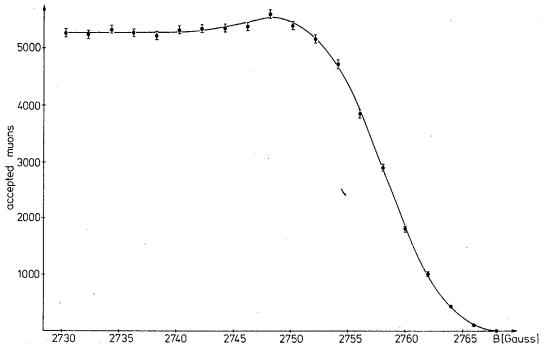

FIG. 13. Predicted number of muons accepted by the spectrometer as a function of the magnetic field. The points with error bars are the results of the Monte Carlo calculation (assumed decay momentum 29.79 MeV/c). The curve represents an "eye fit" through the points, see Sec. VI.

ror bars in Fig. 13. The solid line, which was used in the data analysis, was obtained by first drawing an "eye fit" curve through the points; this curve was stretched or compressed vertically and shifted horizontally with a χ^2-minimization computer program,[13] until the best fit with the Monte Carlo points was obtained.

VII. COMPARISON OF EXPERIMENTAL AND THEORETICAL MUON SPECTRA

In the data analysis the 21 experimental muon spectra (Sec. V) were compared with the theoretical muon spectra. The theoretical curve (Fig. 13) was fitted[13] to the experimental points with two free parameters, namely a normalization factor for the ordinate and the free-muon momentum p_{μ^+}; a small change of p_{μ^+} is equivalent to a horizontal shift of the theoretical curve of Fig. 13.

The final momentum p_{μ^+} was obtained from analyzing the 21 muon spectra separately. However, in order to test with optimum sensitivity whether the experimental and theoretical shape of the spectra agree, we combined the experimental spectra obtained in the same data-taking period and fitted this combined spectrum with the theoretical curve valid for that period (see Fig. 11). Data from different periods were not combined; the theoretical curve is different for each of the six periods because of slight changes of the scintillator size and position, made between periods.

The χ^2 values of the six fits are indicated in Fig. 11 and are satisfactory in all cases. It should be noted that after the normalization of the ordinate there was, for each of the six spectra, only one additional free parameter, namely the decay momentum p_{μ^+}.

The p_{μ^+} uncertainty due to counting statistics for each of the 21 spectra was obtained from the χ^2-minimization program MINUIT.[13] We used the average of the two errors which gives the maximal extension of the curve $\chi^2=\chi^2_{\min}+1$, as the estimate of the standard-deviation uncertainty for p_{μ^+}. This standard deviation was larger than the parabolic[13] error by only a factor of 1.001 on the average. The parabolic error is the square root of the appropriate diagonal element of the error matrix, i.e., it gives the maximal extension, in the direction of the variable p_{μ^+}, of the ellipse where the paraboloid approximating the true χ^2 function cuts the plane $\chi^2=\chi^2_{\min}+1$. In the same way we computed the uncertainty due to the finite number of Monte Carlo events for the theoretical curve (Fig. 13). The combined statistical uncertainty of the final p_{μ^+} value, obtained by quadratic addition of these two contributions, is

$$\Delta p_{\mu^+}(\text{stat}) = 0.0012 \text{ MeV}/c . \quad (6)$$

VIII. FURTHER UNCERTAINTIES AND CORRECTIONS

The remaining contributions to the uncertainty of our p_{μ^+} value are listed in Table I.

A. Measurement of the scintillator and collimator positions

Before and after each running period, the vacuum chamber was placed on the coordinate table of a large milling machine and evacuated. The scintillator and the collimator C (Fig. 2) were viewed through two quartz glass windows with a theodolite set up on the floor as close as possible

TABLE I. Uncertainties of the muon momentum measurement as discussed in Sec. VIII.

Source of uncertainty	Contribution to uncertainty of muon momentum (MeV/c) (standard deviation)
(A) Measurement of the scintillator and collimator positions.	0.000 53
(B) Background subtraction from silicon detector pulse-height spectra.	0.000 34
(C) Calculation of muon energy loss in scintillator.	0.000 17
(D) Calculation of effective muon-source position.	0.000 24
(E) Magnetic-field measurement and stabilization.	0.000 19
Quadratic sum	0.000 72

to the coordinate table. In this way the most critical distance, from the scintillator to the collimator C, was determined. The remaining relevant distances were measured with similar techniques using, e.g., the microscope of the milling machine and a window in the lid of the vacuum chamber above the scintillator. Thermal expansion was studied by heat insulating the vacuum chamber from the coordinate table and heating the chamber with a current lead wrapped around it. During the data-taking runs, the temperature of the vacuum chamber was measured about once an hour using thermistors embedded in the vacuum chamber wall. The coordinate table of the milling machine was calibrated with standard rods, the lengths of which, at 20° C, were measured to a precision of 0.001 mm by the Eidgenössisches Amt für Mass und Gewicht in Bern. The main part of this contribution to the p_{μ^+} uncertainty is due to the scatter of repeated measurements with the theodolite. A detailed discussion of these distance measurements is given in Ref. 8.

B. Background subtraction from the silicon-detector pulse-height spectra

After the subtraction of the accidental background from the silicon-detector pulse-height spectra, there remained on the left of the peak (Fig. 9) a flat background attributed to muons scattered in the collimators (predominantly in the final collimator C).

In our analysis, the good-event count was started three channels below the peak, e.g., in channel 100 in the case of Fig. 9. Scattered muons which lose little energy in the collimators give events in the peak of Fig. 9, i.e., the background in channels 65 to 100 has to be extrapolated under the peak and subtracted. The way in which this was done is illustrated in Fig. 14. This represents our best estimate of the background spectrum; we also did a complete analysis where no events were subtracted under the peak. The result of the first analysis was used as the final value; the difference of the results of the two analyses, 0.000 31 MeV/c, was used as the corresponding contribution to the p_{μ^+} uncertainty. This contribution is small because the scattered muon background has about the same dependence on magnetic field as the good events; see Fig. 15.

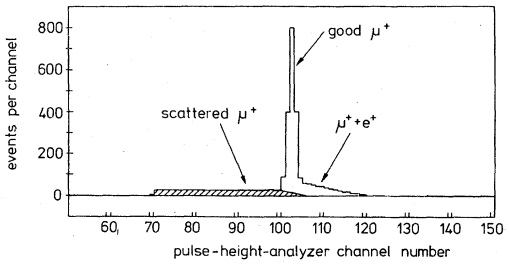

FIG. 14. Schematic diagram of the nonaccidental silicon-detector pulse-height spectrum [cf. Fig. 9 (c)]. The flat background due to muons scattered from the collimators was extrapolated under the peak due to nonscattered muons (channel 103) as indicated, see Sec. VIII B.

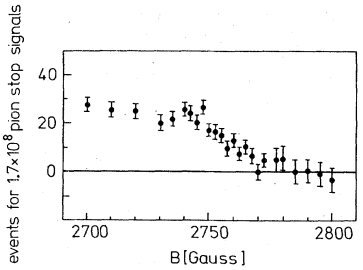

FIG. 15. Number of events due to muons scattered from collimators, as a function of the magnetic field. This number of events was calculated by summing, in the "nonaccidental" spectrum, e.g., Figs. 9 (c) and 10 (c), the events in the channels (I-25) to (I-6), where I is the channel number of the peak (I= 103 in Fig. 9). Because of the similarity in the shape of this spectrum with the "good" spectra of Fig. 11, the subtraction of the background due to scattered muons caused only a small uncertainty of the muon momentum; this is discussed in Sec. VIII B.

The subtraction of the accidental background also led to a small p_{μ^+} uncertainty because of pos-

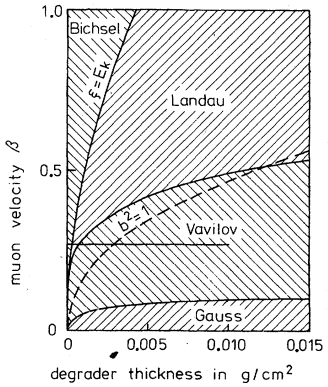

FIG. 16. Regions of validity for energy-loss straggling theories in the case of degraders of carbon or compounds of hydrogen and carbon. In the "Bichsel" region, separated by the curve $\xi = E_K$ (ξ, see Ref. 18; E_K= binding energy of a K-shell electron of carbon = 313 eV), the Vavilov and Shulek theories are not accurate, as discussed in Ref. 17. To the left of the curve $b^2 = 1$, the Blunck-Leisegang (Ref. 16) and Shulek (Ref. 15) corrections are important. The horizontal line at $\beta = 0.27$ indicates the conditions important for this experiment, see Sec. VIII C.

sible inaccuracies in the relative calibration, determined from the α line, of the two pulse-height analyzers used for the two spectra [Figs. 9(a) and 9(b)]. This uncertainty could have been avoided using routing techniques; however, the uncertainty was only 0.000 13 MeV/c; see Ref. 8. The combined uncertainty due to background subtraction, obtained by adding the two contributions in quadrature, is 0.000 34 MeV/c.

C. Calculation of muon energy loss in the scintillator

The theoretical muon spectrum for each running period (Sec. VI) was calculated twice, first using the Vavilov theory[14] of energy loss, then the theory of Shulek *et al.*[15] In this way two p_{μ^+} values were obtained. The average of the two results was used as the final p_{μ^+} value, and the difference of the average from either of the two p_{μ^+} values, 0.000 09 MeV/c, was used as a first contribution to the corresponding uncertainty.

The regions of validity for various energy loss theories are shown in Fig. 16 for the case of the material NE102A used for our scintillator. The horizontal line at $\beta = 0.27$ indicates the conditions important for our experiment. To the left of the curve labeled $b^2 = 1$ (see Ref. 16) the Shulek energy-loss distributions differ strongly from the uncorrected Vavilov distributions. Bichsel[17] has pointed out that to the left of the curve $\xi = E_K$ none of the calculations based on the Laplace transformation (Landau, Vavilov, Shulek) are accurate. Here, ξ is the energy-loss parameter[18]; for the material NE102A, one finds $\xi = (x/\beta^2) \times 83$ keV cm^{2}g, where x is the degrader thickness in g/cm^2. E_K is the ionization potential for the K shell of the carbon atom ($E_K = 313$ eV). At $\beta = 0.27$, the "Bichsel" region (Fig. 16) reaches from zero to 0.003 g/cm^2. In this region the energy-loss distributions for degraders of NE102A were recently calculated[19] by a method similar to that of Bichsel and Saxon.[20] The widths of the resulting distributions[19] and also the widths of the measured distributions[21-23] for conditions in the Bichsel region are between the widths of the Shulek and Vavilov curves; therefore, the uncertainty of 0.000 09 MeV/c discussed above is large enough to include the inaccuracy of the Shulek and Vavilov theories for very small degrader thickness.

Further contributions came from the uncertainties of the effective excitation potential used to calculate the average energy loss for a given path length (0.000 10 MeV/c), and of the numerical methods used in the calculation of the theoretical muon spectrum (0.000 10 MeV/c); see Ref. 8. The combined uncertainty due to energy-loss calculations, obtained by adding the three contributions in quadrature, is 0.000 17 MeV/c.

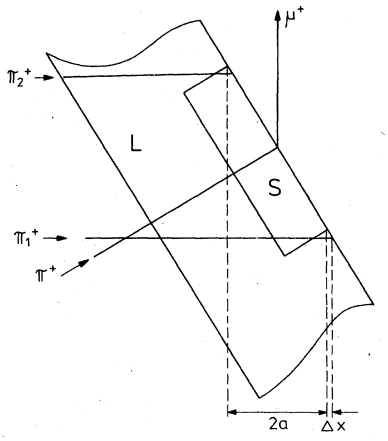

FIG. 17. Schematic diagram of the scintillator (S) and the light guide (L); see Fig. 3. If the average direction of the good pions (π^+) is not perpendicular to the surface of S, there is a shift of the effective μ^+ source position due to edge effects. The pion π_1^+ generates a good signal in S but stops outside, whereas π_2^+ does not generate a good signal but stops inside S, see Sec. VIII D.

D. Calculation of effective muon-source position

The effective position and shape of the muon source in our spectrometer is not exactly defined by the scintillator owing to a number of effects;

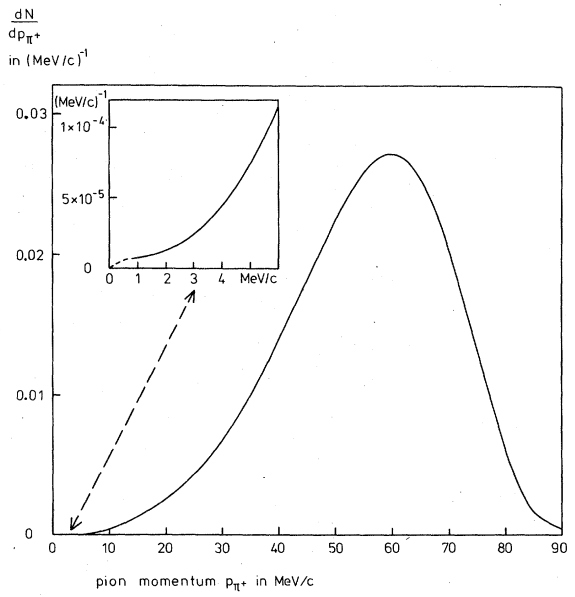

FIG. 18. Momentum distribution of pions leaving the downstream face of the scintillator, calculated as specified in Sec. VIII D from the stopping power. As there are few slow pions, the decay in flight of pions outside of the scintillator only leads to a small p_{μ^+} correction.

First, the slightly inhomogeneous pion-stopping distribution in the scintillator had to be considered; it was determined experimentally and included in the analysis.[8] The uncertainty in the position of the maximum of the measured pion-stop distribution (±1 mm) led to a p_{μ^+} uncertainty of 0.000 09 MeV/c. As a second, more important source of uncertainty, the variation of the pion-stop counting efficiency near the edges of the scintillator had to be taken into account. As illustrated in Fig. 17 there are pions which stop inside the scintillator but do not generate a stop signal (energy loss in the scintillator less than 3.0 MeV); on the other hand, a pion may generate a stop signal but stop in the light guide outside the scintillator. These edge effects lead to a spatial shift in the effective muon-source center if the mean flight direction of the "good" pions deviates from the normal to the face of the scintillator. This mean pion-flight direction was determined from beam scans in the multiwire proportional chamber upstream of the pion degrader (Fig. 2) and at the position of the scintillator, using a Monte Carlo program to trace the pions through the degrader, the fringe field of the magnet, and the scintillator light guide. In this way the mean flight direction of the good pions could be determined with an uncertainty of 1.0°. The deviation of this direction from the normal to the scintillator face led to a correction[8] of the p_{μ^+} values, and the uncertainty of 1.0° gave an uncertainty of 0.000 22 MeV/c for the final result.[8]

As a third effect connected with the shape and position of the effective muon source we had to consider the decay in flight of those pions which generate a pion-stop signal, i.e., lose more than 3.0 MeV in the scintillator, but leave the downstream face of the scintillator. In Fig. 18 the momentum distribution of all pions leaving the downstream face of the scintillator is plotted. A pion-stop signal is generated (energy loss in scintillator more than 3 MeV) if the momentum p_{π^+} is smaller than about 17 MeV/c. The curve of Fig. 18 was obtained according to Ref. 24 from the stopping power of polystyrene as determined experimentally by Sautter and Zimmermann[25] down to an ion velocity of 0.008c (p_π = 1.1 MeV/c); for lower pion momenta the stopping power was estimated from theoretical considerations by Lindhard and Scharff.[26] The total area of the curve of Fig. 18 is unity, so the probability that a pion leaving the scintillator has a momentum below 1 MeV/c is less than 10^{-5}. Only these very slow pions can give rise to a good event, because pions with $p_\pi > 1$ MeV/c hit the wall of the vacuum chamber before the electronically set delay time for a good event (10 nsec; Sec. IV G) had elapsed. The decays in flight produced events mainly if the magnetic field was in the slope region (Fig. 11) near 2760 G. If the good-event number (from stopped pions) near 2730 G is normalized to 1.0, then the average number of events from decay in flight in the slope region is 3×10^{-4} (5×10^{-4}) events for the larger (smaller) scintillator size (see Sec. IV). The cor-

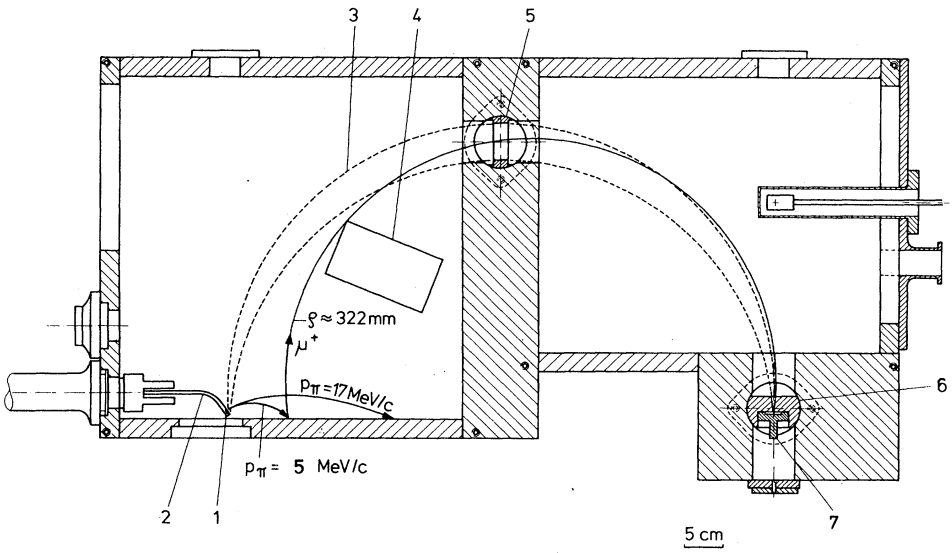

FIG. 19. Trajectories of pions which have generated a good signal in the scintillator (energy loss > 3 MeV) but have not stopped in the scintillator. The momentum range of these pions is $0 < p_\pi \lesssim 17$ MeV/c. (1) scintillation counter, (2) light guide, (3) envelope of good muon trajectories, (4) lead beam blocker, (5) collimator B, (6) collimator C, (7) silicon detector. See Sec. VIII D.

responding p_{μ^+} correction was −0.000 04 MeV/c (−0.000 05 MeV/c). As several approximations were used for the calculation of this very small correction (only one-thirtieth of the total p_{μ^+} uncertainty), we set the corresponding uncertainty equal to the full magnitude of the correction (0.000 05 MeV/c).

Pions from the downstream face of the scintillator may, instead of decaying in flight, return to the scintillator, the light guide, or the wall of the vacuum chamber, see Figs. 19 and 20. From Fig. 19 it is clear that good events of this type can only come from slow pions ($\lesssim 5$ MeV/c). Such pions stop near the surface, and the muons enter the vacuum with almost the full decay momentum. Some events in the magnetic-field region of the slope (Fig. 11) come from such return pions stopped in the scintillator or the light guide to the right. The number of these events, averaged over the slope region, was 2×10^{-4} (1×10^{-4}) of the good-event rate near $B = 2730$ G, for the larger (smaller) scintillator size. The corresponding p_{μ^+} correction was −0.000 03 MeV/c (−0.000 01 MeV/c). Again the p_{μ^+} uncertainty for this small effect was set equal to the magnitude of the correction. The four contributions to the p_{μ^+} uncertainty just discussed (calculation of shape and position of effective muon source) were added in quadrature; the resulting uncertainty was 0.000 24 MeV/c.

E. Magnetic-field measurement and stabilization

The corresponding p_{μ^+} uncertainty arises primarily from the absolute uncertainty of the magnetic-field value measured with the NMR device (standard deviation $= 6\times10^{-6}$; $\Delta p_{\mu^+} = 0.000\,17$ MeV/c). Additional uncertainties were derived from the scatter of repeated determinations of the "effective" field (see Sec. IV E; $\Delta p_{\mu^+} = 0.000\,05$ MeV/c) and from the uncertainty of the spatial position of the reference probe during the data-taking runs[8] ($\Delta p_{\mu^+} = 0.000\,06$ MeV/c). The combined p_{μ^+} uncertainty due to magnetic-field uncertainties is thus 0.000 19 MeV/c.

F. Other effects

A number of other effects have been studied: The pions which stop in the scintillator either behave as positive ions or form pionium.[27] In both cases it can be inferred from the better known behavior of positive muons in a plastic scintillator that the diffusion of the pions through the scintillator is negligibly slow. Pions scattered in the scintillator and reaching the silicon detector are suppressed by the scintillator pulse-height requirement and also by the timing of the scintillator and silicon-detector coincidence circuit (Sec. IV G). The thermal motion of the stopped pions and

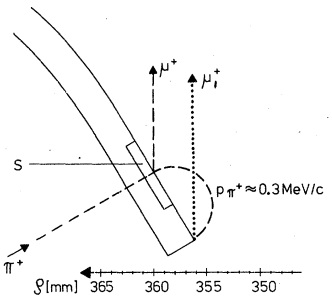

FIG. 20. Same as Fig. 19, but for extremely slow pions. Muons of the type μ_1^+ indicated in the figure cause only a small p_{μ^+} correction and uncertainty because the number of slow pions is small (see Fig. 18).

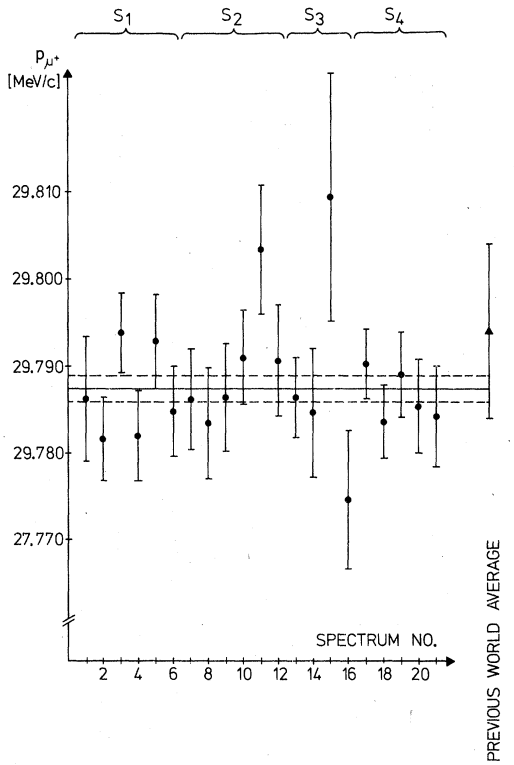

FIG. 21. Results for the muon momentum from stopped pion decay obtained from the 21 muon spectra recorded in the experiment. Error bars include statistical and other uncertainties added in quadrature. Symbols S_i at the top of the graph designate the use of the four different scintillators. Horizontal straight lines indicate the final value with its total uncertainty. The 21 p_{μ^+} values fit the final result with a χ^2 of 23.5 (20 degrees of freedom); uncertainties common to all 21 p_{μ^+} values were not included in this χ^2 value. The previous world average, $p_{\mu^+} = (29.794 \pm 0.010)$ MeV/c, is shown for comparison.

TABLE II. Published results of direct measurements of the muon momentum in pion decay at rest. The quoted uncertainties are standard deviations.

Experiment	Muon momentum (MeV/c)
Barkas *et al.*[a]	29.80 ±0.04
Hyman *et al.*[b]	29.770 ±0.027
Booth *et al.*[c]	29.803 ±0.020
Shrum and Ziock[d]	29.795 ±0.013
This experiment	29.7877 ±0.0014

[a] Reference 30.
[b] Reference 31.
[c] Reference 5.
[d] Reference 32.

the chemical potential in the scintillator, from which the muons had to escape, were also calculated to have a negligible effect on the result.[8]

IX. RESULTS

The p_{μ^+} results derived from the 21 individual muon spectra are displayed in Fig. 21. Their weighted average is

$$p_{\mu^+} = 29.7877 \pm 0.0014 \text{ MeV}/c . \quad (7)$$

The uncertainty due to counting and Monte Carlo statistics (Sec. VII) is 0.0012 MeV/c and the combined uncertainty due to the effects discussed in Sec. VIII is 0.0007 MeV/c. The stated uncertainty of 0.0014 MeV/c (one standard deviation) was obtained by adding the two contributions in quadrature. This p_{μ^+} result includes all data of our earlier publications on this experiment[8,28,29] and is intended to replace the results given there. The slight deviation of the new result (7) from those of Refs. 8 and 29 is due to refinements of the muon energy-loss calculations (Sec. VIIIC) and of the corrections for nonstopped pions (Sec. VIIID).

In Table II published results of direct measurements of p_{μ^+} are listed. Our result is consistent with the earlier values.

We have used the p_{μ^+} value of Eq. (7) to calculate the upper limit for the muon-neutrino mass. The muon and pion masses of Ref. 6, $m_{\mu^+} = 105.659\,46 \pm 0.000\,24$ MeV/c^2, $m_{\pi^-} = 139.5679 \pm 0.0015$ MeV/c^2, were used. Assuming that m_{π^+} is equal to m_{π^-} (CPT theorem) one obtains from Eq. (1) the squared neutrino mass,

$$m_{\nu_\mu}{}^2 = 0.13 \pm 0.14 \text{ (MeV}/c^2)^2 . \quad (8)$$

The uncertainty of $m_{\nu_\mu}{}^2$ (one standard deviation) has been obtained by adding the three contributions given by Eqs. (2)–(4) in quadrature. The contributions of Δm_π and Δp_{μ^+} to $\Delta(m_{\nu_\mu}{}^2)$ are about equal, whereas the contribution of Δm_μ is much smaller.

Following the method recommended by the Particle Data Group,[33] illustrated in Fig. 22, we calculated the upper limit of the muon-neutrino mass. The result is

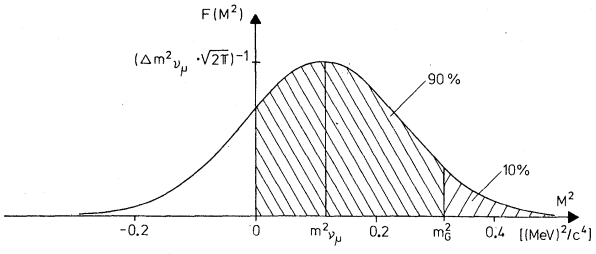

FIG. 22. According to the prescription of the Particle Data Group (Ref. 33) the upper limit m_G of the muon-neutrino mass is calculated from the squares mass $m_{\nu_\mu}{}^2$ and its uncertainty $\Delta(m_{\nu_\mu}{}^2)$ by setting the probability function $F(M^2)$ to zero for $M^2 < 0$, as indicated in the figure.

$$m_{\nu_\mu} \leq 0.57 \text{ MeV}/c^2 \text{ (90\% confidence level)} . \quad (9)$$

This limit is lower than the best previous limit of 0.65 MeV obtained by Clark *et al.*[4] from fits to the $\pi\mu$ mass spectra in $K_L^0 \to \pi^\pm \mu^\mp \nu$ decays using the $V-A$ theory.

As an alternative interpretation, one can use the p_{μ^+} value of Eq. (7) to calculate the mass difference $(m_{\pi^+} - m_{\mu^+})$ or the mass m_{π^+} of the positive pion. For this one uses cosmological calculations based on the big-bang hypothesis. If one assumes that the mean lifetime of the neutrino is greater than or about equal to the age of the universe, one obtains[2] $m_{\nu_\mu} < 40$ eV/c^2. This upper limit is negligibly small for our purpose, and we obtain

$$m_{\pi^+} - m_{\mu^+} = p_{\mu^+} + T_{\mu^+} = 33.9063 \pm 0.0018 \text{ MeV}/c^2 . \quad (10)$$

This value for the mass difference depends only weakly on the muon mass. For the mass of the positively charged pion we obtain

$$m_{\pi^+} = 139.5658 \pm 0.0018 \text{ MeV}/c^2 . \quad (11)$$

This value is consistent with the m_{π^-} value calculated from x-ray lines of pionic atoms,[6] $m_{\pi^-} = 139.5679 \pm 0.0015$ MeV/c^2. Our result is thus in agreement with the prediction from the CPT theorem $(m_{\pi^+} = m_{\pi^-})$. The mass values (10) and (11) represent a considerable improvement. The previous world average for p_{μ^+} (see Fig. 21) gave a π^+ mass uncertainty of 0.013 MeV/c^2.

ACKNOWLEDGMENTS

We wish to thank Professor H.-J. Gerber for his consistent support of our experiment, Professor F.J.M. Farley and Dr. A. Schenck for enlightening discussions, and Dr. C. Amsler, R. Balsiger,

G. Buxton, M. Byrne, S. Cox, Dr. L Dubal, P. Funk, P. Gheno, R. Hausammann, P. House, B. Jost, M. Moser, W. Steffen, R. O. Stemland, and P. Wiederkehr for their help with the preparation, the data taking or the analysis of the experiment. We also thank H. Schürch of the Eidgenössisches Amt für Mass und Gewicht for his kind cooperation. The efficient support of many SIN staff members is gratefully acknowledged.

---

*Present address: Marconi Space and Defence Systems Ltd., Stanmore, Middlesex HA7 4LY, England.
†Present address: Department of Physics, University of Virginia, Charlottesville, Virginia 22901.

[1]R. Cowsik and J. McClelland, Phys. Rev. Lett. 29, 669 (1972).
[2]B. W. Lee and S. Weinberg, Phys. Rev. Lett. 38, 165 (1977).
[3]E. F. Tret'yakov, N. F. Myasoedov, A. M. Apalikov, V. F. Konyaev, V. A. Lyubimov, and E. G. Novikov, Izv. Akad. Nauk SSSR, Ser. Fiz. 40, 2026 (1976) [Bull. Acad. Sci. USSR, Phys. Ser. 40 (No. 10), 1–9 (1976)].
[4]A. L. Clark, T. Elioff, H. J. Frisch, R. P. Johnson, L. T. Kerth, G. Shen, and W. A. Wenzel, Phys. Rev. D 9, 533 (1974).
[5]P. S. L. Booth, R. G. Johnson, E. G. H. Williams, and J. R. Wormald, Phys. Lett. 26B, 39 (1967); 32B, 723 (1970).
[6]Particle Data Group, Phys. Lett. 75B, No. 1 (1978).
[7]R. Frosch and P. Funk, SIN Report No. TM-30-15, 1974 (unpublished).
[8]M. Daum, Ph.D. thesis No. 6269, ETH Zurich, 1978 (unpublished).
[9]*Alpha-, Beta-, and Gamma-Ray Spectroscopy*, edited by K. Siegbahn (North-Holland, Amsterdam, 1965).
[10]SIN-Benützerhandbuch, Sec. IV A, 1972 (unpublished).
[11]R. O. Stemland, SIN Report No. TM-38-01, 1975 (unpublished).
[12]D. R. Hartree, Proc. Cambridge Phil. Soc. 21, 746 (1923).
[13]F. James and M. Roos, CERN 6600 Computer Program Library D506, 1967 (unpublished).
[14]P. V. Vavilov, Zh. Eksp. Teor. Fiz. 32, 920 (1957) [Sov. Phys.—JETP 5, 749 (1957)].
[15]P. Shulek, B. M. Golovin, L. A. Kulyukina, S. V. Medved, and P. Pavlovich, Yad. Fiz. 4, 564 (1966) [Sov. J. Nucl. Phys. 4, 400 (1967)].
[16]C. Blunck and S. Leisegang, Z. Phys. 128, 500 (1950).
[17]H. Bichsel, Phys. Rev. A 9, 571 (1974).
[18]L. Landau, J. Phy. Moscow 8, 201 (1944).
[19]R. Frosch, SIN Report No. TM-37-11, 1979 (unpublished).
[20]H. Bichsel and R. P. Saxon, Phys. Rev. A 11, 1286 (1975).
[21]G. T. Huetter, R. Madey, and S. M. Yushak, Phys. Rev. A 6, 250 (1972).
[22]H. D. Maccabee, M. R. Raju, and C. A. Tobias, Phys. Rev. 165, 469 (1968).
[23]P. V. Ramana Murthy and G. D. Demeester, Nucl. Instrum. Methods 56, 93 (1967).
[24]G. Buxton, S. Cox, and R. Frosch, SIN Report No. TM-37-06, 1977 (unpublished).
[25]C. A. Sautter and E. J. Zimmerman, Phys. Rev. 140, A490 (1965).
[26]J. Lindhard and M. Scharff, Phys. Rev. 124, 128 (1961).
[27]A. Schenck, private communication, 1977.
[28]M. Daum, L. Dubal, G. H. Eaton, R. Frosch, J. McCulloch, R. C. Minehart, E. Steiner, C. Amsler, and R. Hausamman, Phys. Lett. 60B, 380 (1976).
[29]M. Daum, G. H. Eaton, R. Frosch, H. Hirschmann, J. McCulloch, R. C. Minehart, and E. Steiner, Phys. Lett. 74B, 126 (1978).
[30]W. H. Barkas, W. Birnbaum, and F. M. Smith, Phys. Rev. 101, 778 (1956).
[31]L. G. Hyman, J. Loken, E. G. Pewitt, M. Derrick, T. Fields, J. McKenzie, I. T. Wang, J. Fetkovich, and G. Keyes, Phys. Lett. 25B, 376 (1967).
[32]E. V. Shrum and K. O. H. Ziock, Phys. Lett. 37B, 115 (1971).
[33]T. G. Trippe, private communication, 1976.